ERA-40 Project Report Series

No. 26 Assessing land-surface-atmosphere coupling in the ERA-40 reanalysis with boreal forest data

---

Alan K. Betts, John H. Ball, Alan G. Barr, T. Andy Black,
J. Harry McCaughey and Pedro Viterbo

Series: ECMWF ERA-40 Project Report Series

A full list of ECMWF Publications can be found on our web site under:
http://www.ecmwf.int/publications/

Contact: library@ecmwf.int

European Centre for Medium Range Weather Forecasts
Shinfield Park, Reading, RG2 9AX, England

ERA-40 Project Report Series No. 26

Assessing land-surface-atmosphere coupling in the ERA-40 reanalysis with boreal forest data

Alan K. Betts[1], John H. Ball[1], Alan G. Barr[2]
T. Andy Black[3] J. Harry McCaughey[4]
and Pedro Viterbo[5]

August 2006

[1] Atmospheric Research, Pittsford, VT 05763, USA
[2] Climate Research Branch, Meteorological Service of Canada,
11 Innovation Blvd., Saskatoon, SK, Canada S7N 3H5
[3] Faculty of Land & Food Systems, Univ. of British Columbia,
Vancouver, BC, Canada,
[4] Dept of Geography, Queens University, Kingston, ON, Canada
[5] ECMWF, Reading, UK [current address: Instituto de Meteorologia, Rua C
Aeroporto, 1749-077 Lisboa, Portugal]

In press Agric. For. Meteorol., BERMS special issue

Abstract

This analysis uses long time-series of daily mean data from the three BERMS flux sites in central Saskatchewan to explore biases in ERA-40 at a close-by grid-point, and to study the relationships between surface variables and fluxes and cloud cover in the observed and model data sets. On the seasonal timescale the biases in ERA-40 of temperature and humidity are small, but the model has a high bias in evaporation, and except in mid-summer a low bias of reflective cloud, which gives a high bias in the surface downward net shortwave flux. In summer, on days with high observed cloud cover, the model has too little cloud, and a corresponding high sensible heat flux and a warm, dry bias; while on summer days when observed cloud is lower, the model biases are generally reversed. The internal relationships between near-surface relative humidity, linked to the mean lifting condensation level, cloud cover and the surface radiation fluxes are however very similar in model and data. Although cause and effect cannot be determined from these biases alone, given the complexity of the interactions, they suggest possible errors in both the land-surface model and the atmospheric cloud parameterizations.

1. Introduction

Global models are used both to assimilate global data sets and to make weather forecasts out to the seasonal timescale, as well as for simulations of the earth's climate. The horizontal resolution in the European Centre for Medium-range Forecasts (ECMWF) model for 10-day global forecasts is now about 25 km, with 91 levels to resolve the atmosphere in the vertical. However, despite the increases in resolution in recent decades with increased computational power, many physical processes are still parameterized in global models; in particular, cloud microphysical and convective processes, boundary layer and land-surface processes, and the sub-surface hydrology. For the most part, these parameterized physical processes cannot be evaluated separately since they all interact in determining for example the surface energy and water fluxes in a model. Unfortunately at present, models differ widely in these interactions at the land-surface (Koster et al., 2004; Dirmeyer et al., 2005), and in the local feedbacks between evaporation and precipitation, and this limits our ability to predict weather and climate. Research quality data from surface flux towers provide a set of observables that can be used to evaluate how this land-surface-atmosphere interaction behaves for a particular climate regime; and evaluate whether it is well represented by a model. In this paper, we compare data from the recent ECMWF reanalysis model, which is generally known as ERA-40 (Uppala et al., 2005), with data from the three mature forest Boreal Ecosystem Monitoring Study (BERMS) sites in central Saskatchewan, which are part of the Fluxnet-Canada Research Network (FCRN). None of the FCRN data from these sites entered the reanalysis, so it is an independent assessment of ERA-40 for this region, as well as an evaluation of the land-surface-cloud coupling at these latitudes in ERA-40. Like other models, the ECMWF model is continually evolving. In the mid-1990s, there were significant errors in the seasonal cycle of temperature in the ECMWF model, and in particular a cold bias in winter at high latitudes (Betts et al., 1998a). A new tiled land-surface model was developed (Van den Hurk et al., 2000; Betts et al., 2001), which included a forest tile with snow under the canopy, using data from the Boreal Ecosystem-Atmosphere Study (BOREAS). This land-surface model was incorporated into ERA-40, which was a retrospective analysis for the period September1957-August 2002, using the historic archive of observations with a frozen model. The horizontal resolution of ERA-40 is about 120 km. Because of their global coverage, reanalysis data are used for a very wide range of purposes. This evaluation of ERA-40 is local to a small region of the boreal forest, where we have long time series of research quality data. Betts et al. (2003) evaluate ERA-40 over the Mackenzie river basin, and Betts et al. (2006b) intercompare the near-surface global data sets from

reanalyses, in-situ and satellite observations, that have been compiled as part of the International Land-Surface Cloud Climatology Project.

The three BERMS sites, stands of mature aspen, jack pine and black spruce, were originally instrumented with walk-up towers for the BOREAS experiment, and data was collected during 1994 and 1996 (Blanken et al., 1997; Baldocchi at et al., 1997; Jarvis et al., 1997). For BERMS, these towers were fitted with essentially identical instrument systems to monitor the meteorology, radiation fields and surface fluxes continuously year round. The data from these sites, along with additional satellite sites in younger forest stands following disturbance by fire and harvesting, have been used to evaluate the carbon and water cycles of contrasting forest types (Blanken et al. 2001; Arain et al., 2002; Griffis et al., 2003; Kljun et al., 2006), to characterize the climatic and biophysical factors that control inter-annual variability in net ecosystem productivity (Black et al., 2000; Barr et al., 2002; Barr et al., 2004; Barr et al., in press; Griffis et al., 2004)), to study the forest moisture balance (Barr et al., 2000, Arain et al., 2003), to investigate the impact of fire and harvesting on the carbon, water and energy cycles (Amiro et al., 2005; Amiro et al., submitted), to evaluate process models (Arain et al., 2002; Chen et al., 2003; Grant et al., 2005; Ju et al., 2006) and remote sensing products (Drolet et al., 2005).

In this paper we take an hourly timeseries from ERA-40 for a grid-point close to the three mature forest BERMS sites in central Saskatchewan, and use the data from these three flux tower sites to evaluate the model near-surface fluxes and meteorology. We will use daily mean values to look at biases between the BERMS data and ERA-40, and at the relationships between variables in the observed and model data sets, which are important to the model climate over the forest.

2. Data used and analysis framework

Figure 1 shows the location of the three BERMS flux towers in central Saskatchewan and the ERA-40 gridbox that we used for our comparison. Table 1 gives the latitude, longitude and elevation of the sites and the center of the ERA-40 gridpoint. We shall refer to the BERMS sites by their abbreviations: OA for the old aspen site; OBS for the old black spruce site and OJP for old jack pine. The two conifer sites, OBS and OJP are only about 29 km apart and within the model gridbox, while OA is some 81 km to the southwest of OBS, and slightly outside the gridbox. To give context to the model evaluation, we also intercompare the three BERMS sites, generally taking OBS as the reference site. Time-series at the closely-spaced conifer sites, OBS and OJP, are very similar.

Table 1: Location of the BERMS sites

Site	Latitude, Longitude	Elevation (m)
Old Aspen: OA	53.629 ^{o}N, 106.2 ^{o}W	590
Old Black Spruce: OBS	53.985 ^{o}N, 105.12 ^{o}W	590
Old Jack Pine: OJP	53.916 ^{o}N, 104.69 ^{o}W	523
ERA-40: grid-point center	54.392 ^{o}N, 105.0 ^{o}W	464

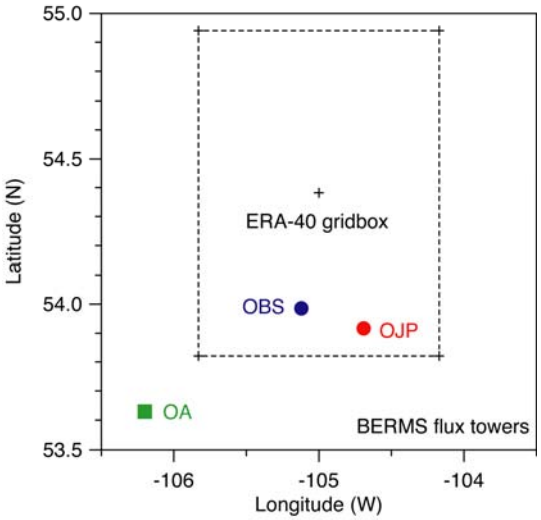

Figure 1 Relative location of BERMS flux sites and ERA-40 gridbox (shown dotted).

2.1 ERA-40 model timeseries

The grid-point timeseries from ERA-40 is hourly mean fluxes and instantaneous hourly meteorological variables derived from 24 h forecasts from each day's 0000 UTC analysis. From this file, we derived a file of daily mean values. Unfortunately ERA-40 ended on August 31, 2002 (and the next ongoing reanalysis is not yet available), while the BERMS data continues after this date, but we have some years of overlap. This is a special hourly research archive from ERA-40 (Kållberg et al., 2004; Betts, 2004), and we have only the single grid-point shown in central Saskatchewan (which was included for comparison with the OBS site); so we do not have the grid-point which includes the OA site.

The ERA-40 tiles land-surface model has 6 tiles (bare soil, high vegetation, low vegetation, high vegetation with snow beneath, snow on low vegetation and a canopy interception layer). There is a coverage map of vegetation types, divided in 17 broad categories; and this gridpoint is 97.6% evergreen needleleaf trees and 2.6% cropland/mixed farmland. The land surface parameters, such as minimal stomatal resistance, leaf area index and rooting depth vary with vegetation type. Following Jarvis (1976), canopy transpiration is controlled by a resistance which is a function of incoming shortwave radiation, leaf area index (LAI), (unfrozen) soil water, atmospheric vapor pressure deficit and a minimum stomatal resistance, which is specified for each vegetation type. For evergreen needleleaf trees, LAI is 5 and the minimum stomatal resistance is 500 s m^{-1}. Maximum canopy interception of rain is a function of LAI. Full details and the parameter sets of the land-surface model is given in Van den Hurk et al. (2000). This land model has limitations: it has no seasonal cycle of LAI, important in the representation of the seasonal cycle of crops and deciduous species, and only a single clay-loam soil type, which is a poor representation of the complex soils of the boreal forest. This model is still part of the operational ECMWF forecast system in 2006, although improvements are under development. The full documentation on the ERA-40 model, its physical parameterizations, numerics and data assimilation, is very extensive; and is available at http://www.ecmwf.int/research/ifsdocs/CY23r4/index.html. A report series evaluating ERA-40 is available at http://www.ecmwf.int/research/era/Products/.

2.2 BERMS data

The BERMS sites are equipped with nearly identical instrument packages, with common calibration and flux processing protocols. For this comparison, we compare data collected above the forest canopy (nominally at 39 m for OA, 25 m for OBS and 28 m for OJP) with the ERA-40 surface fluxes and meteorological data from the lowest model level, about 10m above the surface. The mean canopy heights at the three sites are: OA, 21 m; OBS, 11 m and OJP, 14 m. The basic dataset is 30-min means for the meteorological, radiation and flux data, and our analysis period is 1997-2004. There are measurements of momentum, sensible and latent heat and CO_2 flux for OA for this whole period, while for OBS flux measurements start in late April, 1999, and for OJP in mid-August 1999. The flux data and the four-way net radiation data (shortwave radiation fluxes measured by Kipp and Zonen CM11 pyranometers; and longwave fluxes by Eppley PIR pyrgeometers) have been gap-filled, but a few percent of the data are missing at each site. The primary air temperature (T) and relative humidity (RH) sensors were Vaisala HMP-35CF probes, which were later replaced with HMP-45C probes. The BERMS sites have some redundant instrumentation above the canopy, and these were used to fill gaps in the downward shortwave radiation and the T and RH time-series at each site when available. In general in our analysis of daily means, we excluded days where more than two 30-min values (of the 48 in a daily mean) were missing.

The BERMS flux sites measure pressure, P (at 2-m); T, and RH above the canopy. We corrected P hydrostatically to the above-canopy level. From these variables we computed mixing ratio, Q, and the pressure height to the lifting condensation level, P_{LCL}. For many conditions, P_{LCL} is a good estimate of boundary layer cloud-base. Figure 2 shows that P_{LCL} is primarily a function of RH.

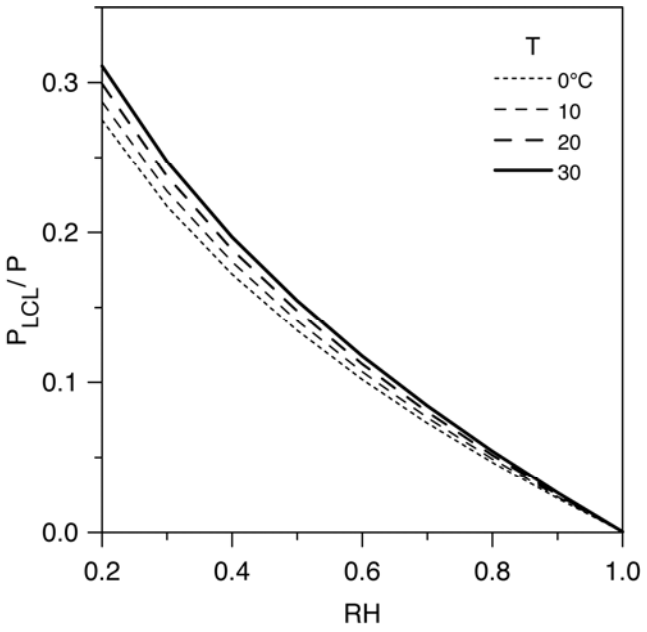

Figure 2: Relation of near-surface RH to pressure height to LCL, scaled by pressure, as a function of T.

2.3 Surface energy balance

The surface energy balance (SEB) can be written

$$SW_{dn} - SW_{up} + LW_{dn} - LW_{up} = SW_{net} + LW_{net} = R_{net} = H + \lambda E + G \ (+ \text{residual}) \qquad (1)$$

where the suffixes denote the downward, upward and net shortwave (SW) and longwave (LW) radiation fluxes. H and 8E are the surface sensible and latent heat fluxes, and G is the storage in the ground, biomass and by photosynthesis/respiration. The model energy balance is closed, but the data have a residual (see later). In the cold season, the residual term includes two terms which were not measured; heat storage in the snow pack and the energy associated with freeze-thaw events in the snowpack and soil. In the warm season, the residual term quantifies the lack of energy balance closure, including errors in the radiation measurements.

2.4 Analysis concepts

Following Betts (2004) and Betts and Viterbo (2005), our analysis will average over the diurnal cycle and look at relationships between daily mean values, to assess systematic biases that may have important impacts on the model climate over the forest. For most variables we will also show the seasonal timescale. The heterogeneity of the landscape has a significant impact on the surface albedo and the evaporative fraction, EF (defined as $\lambda E/(H + \lambda E)$, but the atmospheric boundary layer (BL) plays an important role in averaging over the landscape, as advection at 4 ms^{-1} traverses 14.4 km h^{-1}. During the daytime in unstable conditions, vertical mixing typically closely couples the near-surface variables to the much deeper sub-cloud layer, and convective BL. The BERMS sites are close to the southern edge of the boreal forest in Saskatchewan, but we have not filtered the data for wind direction. We have not accounted for latitudinal gradients except in the computation of clear-sky SW_{dn}. The reanalysis represents quite well the day to day synoptic variability (even though none of the BERMS data were inserted), so when we are comparing observations directly with ERA-

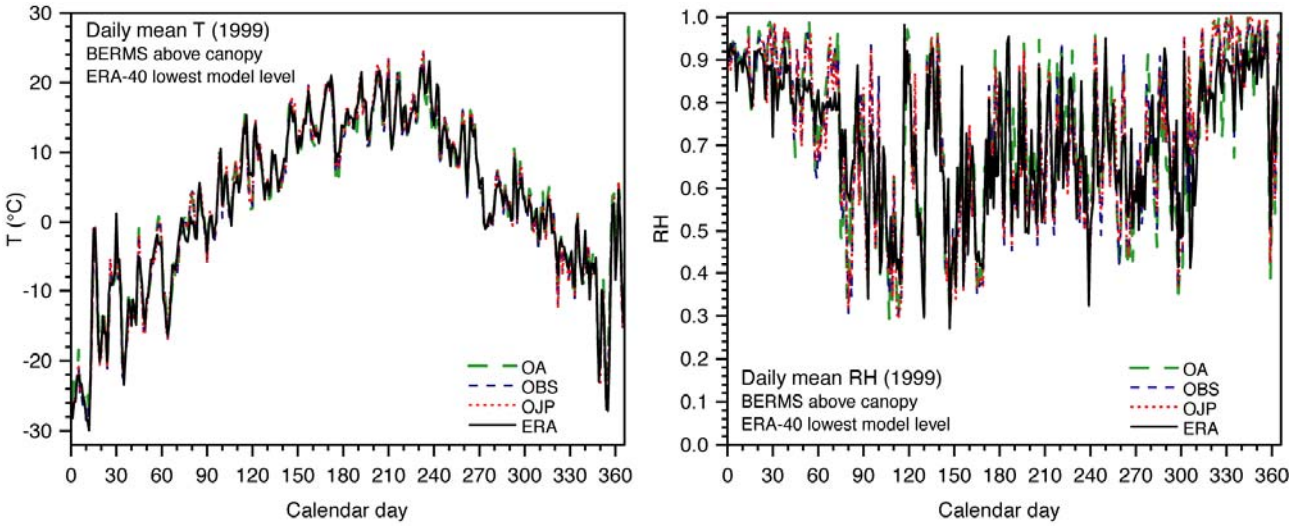

Figure 3: Comparison of ERA-40 (lowest model level) with BERMS (above canopy) annual cycle of temperature (upper) and (lower) relative humidity (RH) for 1999.

40, we use the same time periods. To look at intersite differences and the structure of the ERA-40 biases, we shall stratify the data into bins of observed RH, and observed cloud cover. The near-surface RH is linked to the height of the LCL (see Figure 3), and therefore to the processes that control the equilibrium of the mean BL on daily timescales. Cloud cover, which we quantify as a cloud albedo (see later), has a direct impact on all the downward radiative fluxes and on sensible heat flux.

3. Comparison of above canopy temperature and humidity with ERA-40

3.1 Annual cycle comparison for 1999

Figure 3 compares the annual cycle of daily mean T and RH for 1999 for ERA-40 (about 10-m above surface) and the three BERMS sites (about 15 m above canopy). Below freezing we show RH with respect to ice saturation. For T (upper panel), the three BERMS sites agree quite closely and ERA-40 is within ±2K. The reanalysis has no obvious systematic bias of T in summer or winter (an earlier version of this model had a large cold bias in winter, see Betts et al., 1998a). In RH, the differences in mean RH between reanalysis and the BERMS sites are at times larger (±10%), but on the annual timescale any systematic bias is very small.

3.2 Comparison of daily data between sites and with ERA-40

We now look at the intersite differences in daily mean T and RH, and compare with the corresponding ERA-40 daily means. OBS is chosen as the reference site. Figure 4a) and b) show daily mean T and RH for OJP plotted against OBS, along with the 1-to-1 lines (dashed) and the linear regression lines (solid). The middle panels c) and d) are the corresponding plots for OA against OBS. The two conifer sites (top panels), which are only 29km apart (see Figure 1) agree very closely in T (R^2=0.998) and RH (R^2=0.978). The mean difference of (OJP-OBS) for T= 0.28 ± 0.53K and for RH=0.6 ± 2.8% (see Table 2).The correlation between OBS and OA (which is about 81km from OBS and has a deciduous canopy) is weaker, especially in RH, but the bias is small. Because these intersite differences in T and RH are quite small and largely unbiased (see Table 2), we generated a mean BERMS timeseries of T and RH by simply averaging daily mean values. Where an individual site had missing data, the remaining sites were averaged. Panels e) and f) shows ERA-40 plotted against this BERMS mean. The correlation is lower (R^2=0.984 for T and 0.756 for RH) than between sites, and the regression line suggests that ERA RH has a high bias of RH at low RH and a low bias at high RH (see later). Table 2 summarizes the mean differences and the regression lines. The mean difference of (ERA-BERMS) for T= 0.13 ± 1.61K and for RH= -0.2 ± 9%.

Table 2: Mean differences and correlation of T and RH between BERMS sites and ERA-40

Difference	Mean and SD	Regression on OBS	R^2
ΔT: OJP-OBS	0.28 ± 0.53	T:OJP = 0.24 + 1.010*T:OBS	0.998
ΔT: OA-OBS	0.30 ± 1.01	T:OA = 0.36 + 0.976*T:OBS	0.994
ΔT: ERA-BERMS	0.13 ± 1.61	T:ERA = 0.17 +0.986*T:BERMS	0.984
ΔRH: OJP-OBS	0.006 ± 0.028	RH:OJP =-0.008 + 1.003*RH:OBS	0.978
ΔRH: OA-OBS	-0.010 ± 0.063	RH:OA = 0.022 + 0.954*RH:OBS	0.893
ΔRH: ERA-BERMS	-0.002 ± 0.090	RH:ERA = 0.189 +0.732*RH:OBS	0.769

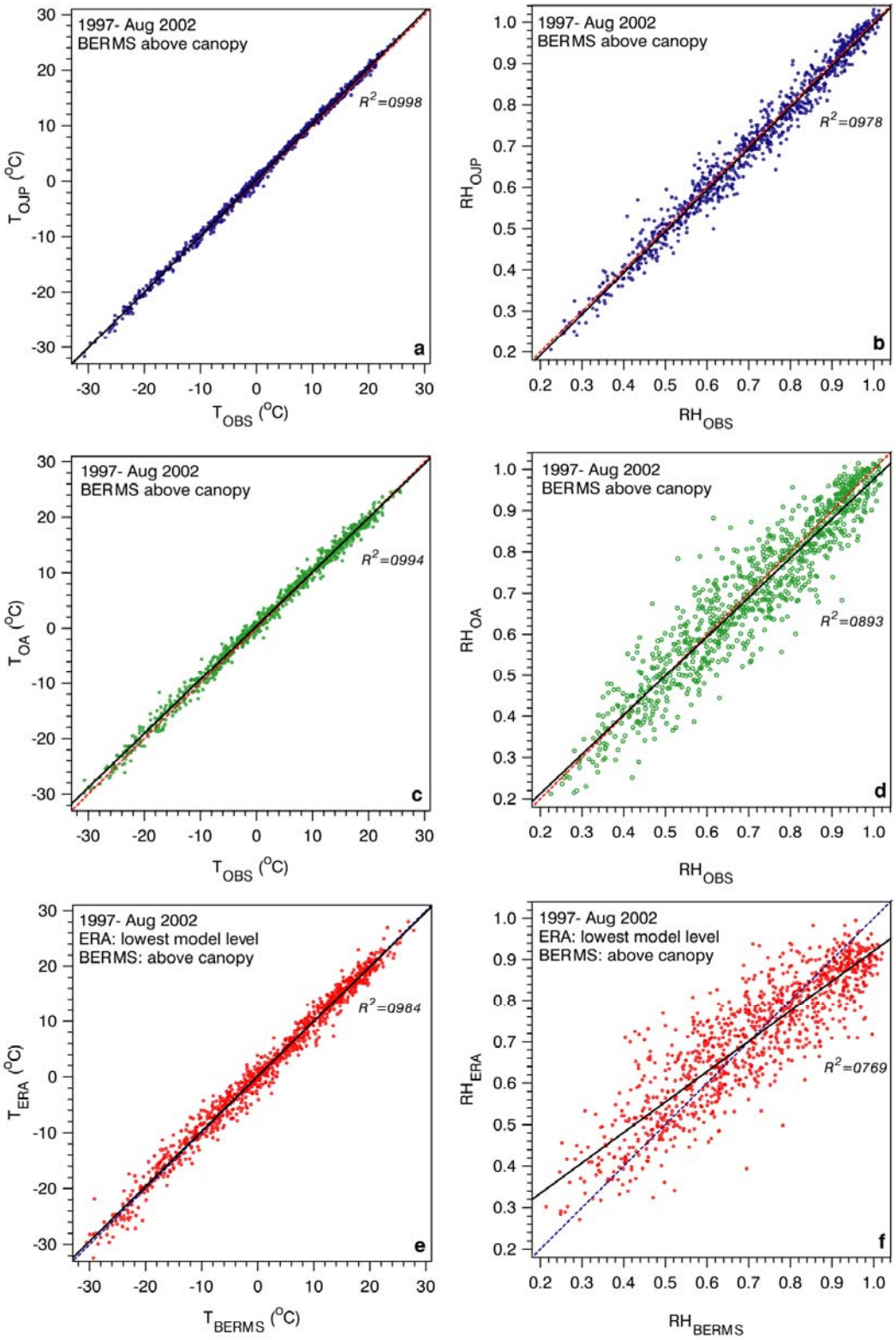

Figure 4: Relationship of daily mean temperature at OJP, OA and for ERA-40 against OBS (left panels) and RH (right panels).

3.3 Mean annual cycle of T and RH

Figure 5(a) shows the mean annual cycle of BERMS temperature, and the mean bias of ERA-40 from the BERMS mean on a greatly expanded right-hand scale. Figure 5(b) is the corresponding plot for RH. The standard deviations shown are the interannual variability of the monthly means. The ERA-40 bias of monthly mean T is very small (< ±0.5°C and comparable to its standard deviation); far less than the interannual variability of mean T, which is largest in winter. This temperature bias is smaller than that found by Betts et al (2003) (of order +2K in winter and -1K in summer) in a comparison of ERA-40 against operational data for the Mackenzie river basin. BERMS mean RH has a minimum and also the largest interannual variability in spring, when evaporation is low (see section 4.5 later), and a maximum in December. ERA-40 has a few percent moist bias in RH in summer and a dry bias of order -5% in winter.

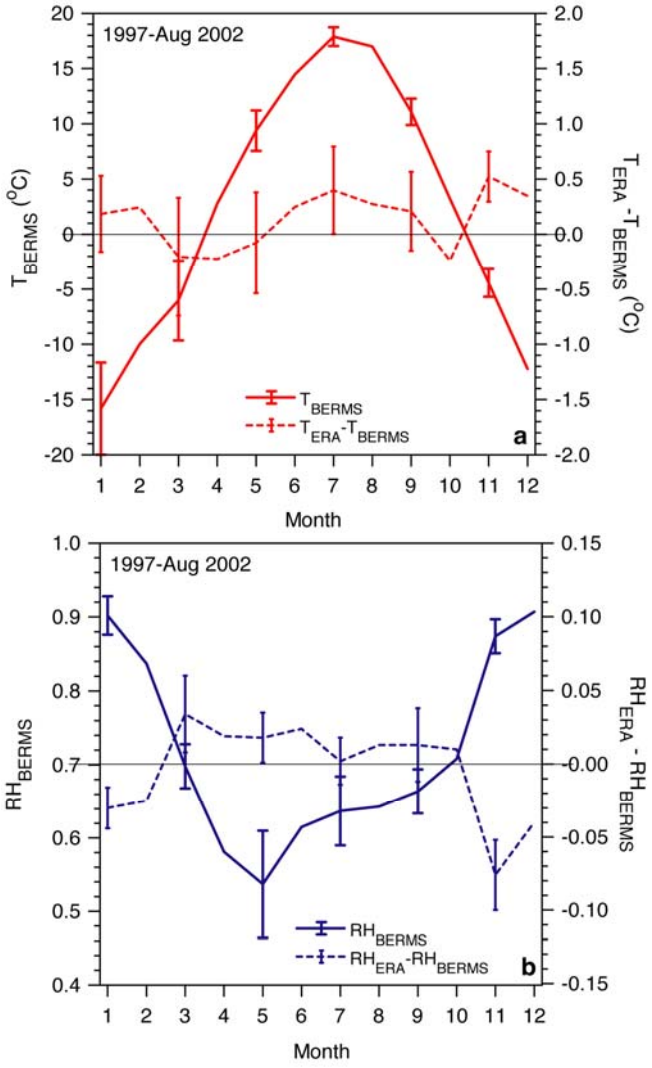

Figure 5: (a) BERMS mean annual cycle of T and ERA-40 T bias, (b) as (a) for RH.

3.4 RH stratification of differences in T and RH

The near-surface RH is linked to the height of the LCL (see Figure 2), and therefore to the processes that control the equilibrium of the BL on daily timescales, so we used 0.1 bins of BERMS mean RH to stratify the data. Figure 6 shows the intersite differences and the ERA-40 biases of RH and T (some selected representative standard deviations are shown). For ERA-40, OBS and OJP we partitioned the year into October-March (cold season months) and April-September (warm season). For OA (middle panel) we separated only the summer months, June to August, of the growing season from the rest of the year. Panel a) shows that for the warm season, OJP is generally slightly warmer (+0.40±0.44K) and drier (-0.9±2.8%) than OBS. For the cold season these biases are smaller. For OA in panel b), in the summer when transpiration is high, OA is generally slightly cooler (-0.26±0.77) and moister (1.6±6.2%) than OBS; but the biases reverse in the other seasons, when OA is warmer and drier. The lower panel c) shows the biases of ERA from the BERMS mean. Not only are the biases much larger (note the doubled scale), but they have a clear structure in both cold and warm seasons as a function of mean RH. At low RH, ERA-40 has a cool, moist bias, which reaches (-1.6K, +9%). This changes to a warm, dry bias, reaching (+1.4K, -4%) at high RH. This bias pattern of RH was already suggested by Figure 4(f). None of the BERMS sites show much variation of their bias from OBS with RH, so this is clearly an error in the model. We shall see in later figures that there are associated biases in cloud cover. It appears that the model physics are effectively damping the observed range of the BL RH, even though the mean biases shown in Figure 5 are relatively small on a seasonal timescale.

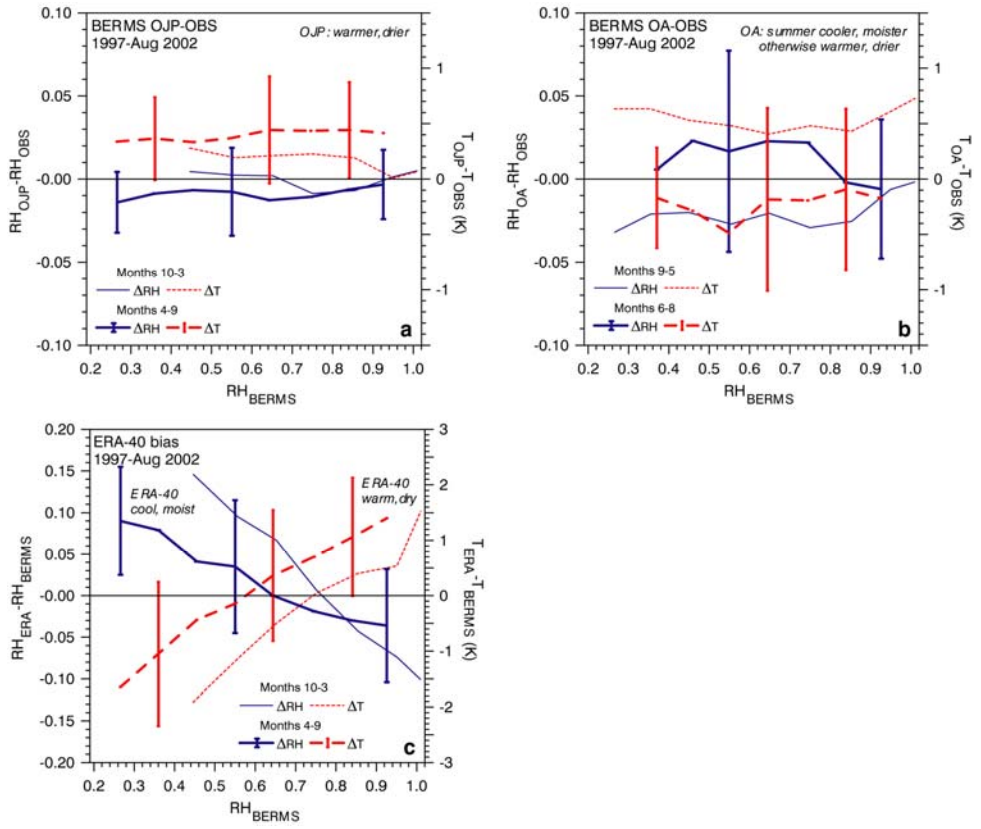

Figure 6: Difference in RH and T as a function of mean BERMS RH for a) OJP-OBS, b) OA-OBS, and c) ERA-BERMS.

4. Surface energy budget comparison

4.1 Daily mean incoming and net radiation fluxes for BERMS and ERA-40

Table 3 shows the statistics of the comparison of SW_{dn}, LW_{dn}, SW_{net}, LW_{net} and R_{net} for OJP, OA with OBS, and ERA-40 with the BERMS mean. Once again OBS and OJP, which are only 29km apart, agree more closely than do OA and OBS, but the intersite differences are small. The mean difference (OJP-OBS) for SW_{dn} = -0.7 ± 17.0 Wm^{-2} and for LW_{dn} = 3.1 ± 6.6 Wm^{-2}; while for (OA-OBS) the mean difference for SW_{dn} = 2.7 ± 26.3 Wm^{-2} and for LW_{dn} = 2.5 ± 11.2 Wm^{-2}. This suggests both excellent calibration of the SW and LW instruments, and little mean atmospheric variability between sites. We again generated a mean BERMS timeseries by simply averaging daily mean values of SW_{dn} and LW_{dn}. Where an individual site had missing data, the remaining sites were averaged. The correlation of ERA-40 with the BERMS mean is again poorer than the intersite comparisons, as model and data have cloud field differences (see section 4.3 later), but the mean bias is small. We show also the statistics of the comparison of SW_{net}, LW_{net} and R_{net} for OJP, OA and OBS, because the regression lines and the mean differences are of interest for climatological comparisons (Betts et al., 2006a). As before, the correlation is largest for the nearby conifer sites. However, compared to OBS, OJP has a slightly smaller SW_{net}, because its surface albedo is higher (see Figure 9 later), and a slightly larger outgoing LW_{net}, because its surface temperature is slightly higher (Figure 6). Compared to OBS, OA also has a smaller SW_{net}, because of a higher surface albedo (see Figure 9 later), and slightly larger outgoing LW_{net}. For much of the year, OA also has a slightly warmer temperature (Figure 6). Consequently, R_{net} is larger at OBS than the other two sites (see Figure 10b later). The downward fluxes are affected by atmospheric heterogeneity, and the upward fluxes depend on the heterogeneity of the landscape, but again it is useful to construct a BERMS mean for the three sites. ERA-40 has a slightly lower SW_{net}, greater outgoing LW_{net} and smaller R_{net} than the BERMS mean. The correlation of ERA-40 with the BERMS

Table 3 Mean differences and correlation of radiation fluxes.

Difference	Mean and SD	Regression on OBS	R^2
SW_{dn}: OJP-OBS	-0.7 ∀ 17.0	SW_{dn}:OJP = 2.2+ 0.979*SW_{dn}: OBS y	0.970
SW_{dn}: OA-OBS	2.7 ∀ 26.3	SW_{dn}:OA = 8.3 + 0.96*SW_{dn}: OBS	0.927
SW_{dn}: ERA-BERMS	0.5 ∀ 38.0	SW_{dn}:ERA = 10.7 + 0.928*SW_{dn}:BERMS	0.849
LW_{dn}: OJP-OBS	3.1 ∀ 6.6	LW_{dn}:OJP = 4.1 + 0.996*LW_{dn}: OBS	0.986
LW_{dn}: OA-OBS	2.5 ∀ 11.2	LW_{dn}:OA = 15.1 + 0.953*LW_{dn}: OBS	0.960
LW_{dn}: ERA-BERMS	0.5 ∀ 16.5	LW_{dn}:ERA = -14.8 + 1.056*LW_{dn}:BERMS	0.928
SW_{net}: OJP-OBS	-3.2 ∀ 16.0	SW_{net}:OJP = 0.7 + 0.970*SW_{net}: OBS	0.968
SW_{net}: OA-OBS	-6.8 ∀ 24.2	SW_{net}:OA = 6.5 + 0.895*SW_{net}: OBS	0.926
SW_{net}: ERA-BERMS	-1.5 ∀ 33.3	SW_{net}:ERA = 9.3 + 0.912*SW_{net}: BERMS	0.853
LW_{net}: OJP-OBS	-0.3 ∀ 6.7	LW_{net}:OJP =-1.3 + 0.982*LW_{net}: OBS	0.939
LW_{net}: OA-OBS	-1.4 ∀ 10.5	LW_{net}:OA = -5.1 + 0.931*LW_{net}: OBS	0.853
LW_{net}: ERA-BERMS	-3.4 ∀ 15.4	LW_{net}:ERA = -15.8+0.770*LW_{net}:BERMS	0.683
R_{net}: OJP-OBS	-3.6 ∀ 14.0	R_{net}:OJP = -0.4 + 0.946*R_{net}: OBS	0.962
R_{net}: OA-OBS	-7.2 ∀ 20.5	R_{net}:OA = 1.2 + 0.884*R_{net}: OBS	0.918
R_{net}: ERA-BERMS	-4.9 ∀ 26.2	R_{net}:ERA = -4.0 + 0.987*R_{net}:BERMS	0.868

mean for the net fluxes is again not as good as the correlation between sites, but the mean differences are still less than 5 W m^{-2}.

4.2 Clear-sky radiation fluxes and 'cloud albedo'

The surface SW_{net} flux is determined by the clear-sky fluxes (which depend greatly on the solar zenith angle), the cloud cover and the surface albedo. It is convenient to uncouple these effects by defining a SW 'cloud albedo' (Betts and Viterbo, 2005), as a measure of the fraction of the downward clear-sky SW flux (SW_{dn}(clear)) that is reflected or absorbed by the cloud field above

$$\alpha_{cloud} = [SW_{dn}(clear) - SW_{dn}] / SW_{dn}(clear) \quad (2)$$

It is not strictly an albedo, because it includes the cloud-absorbed component, but the reflection by the clouds is the dominant term. The non-dimensional surface SW_{net} can be written in the symmetric form

$$SW_{net} / SW_{dn}(clear) = (1-\alpha_{surf})(1-\alpha_{cloud}) \quad (3)$$

where the surface albedo $\alpha_{surf} = SW_{up} / SW_{dn}$. In this scaled form, we see clearly the comparable roles of the surface albedo and the 'cloud albedo' in reducing the surface SW_{net}. The surface albedo varies with vegetation and the seasons, especially with snow cover; while the cloud albedo varies on daily timescales, depending on BL and atmospheric processes. This 'cloud albedo' is an observable in the sense that it can be derived from the BERMS SW_{dn} measurements, if we know SW_{dn}(clear). It is also easily derived from satellite data, as in the well-known methods for deriving the surface radiation budget (Pinker et al., 2003). For the ERA data, it is straightforward to use equation (2) to compute the $\forall_{cloud}$ from the clear-sky flux computed by the model.

Figure 7(a) compares the daily mean BERMS SW_{dn} fluxes (the scattered dots) and the model clear-sky fluxes (SW_{dn} (ERA-clear) as a band of crosses. In summer, the ERA clear-sky fluxes, which have a small spread depending on the atmospheric composition and structure, are a representative upper 'clear-sky' bound on the BERMS SW_{dn} fluxes. The difference, SW_{dn} - SW_{dn} (clear) is just the so-called surface SW cloud forcing, directly related to α_{cloud} though (2). In winter, however, the upper envelope of the BERMS data is as much as 15 Wm^{-2} (about 30%) higher than the ERA clear-sky fluxes, a clear incompatibility between the model clear-sky fluxes and the BERMS observations. Instrumental calibration and accuracy is an issue in winter with cold temperatures and high solar zenith angles. In addition, ice lenses can sometimes form on the dome of the pyranometer, and give an erroneously high measurement. The model computation of the clear-sky flux may of course have errors, but it is very unlikely that they are this large. Another possible reason for the discrepancy is that the mean solar elevation for the ERA gridpoint is about 0.5° lower because of the higher mean latitude (Figure 1). We computed the impact of solar geometry by fitting a seasonal curve to the ratio of the clear-sky fluxes at the ERA grid-point and the adjacent grid-point to the south. We found by interpolation to the three BERMS sites that the impact on the mean at the winter solstice was only a 7.6% increase in the downward clear-sky flux, much too small to explain a 30% bias. So to compute α_{cloud} for the BERMS sites, we use a seasonal weighting function to adjust the ERA clear-sky fluxes in winter to make them compatible with the upper bound of the BERMS SW_{dn} fluxes. The details are given in the Appendix. The upper envelope in Figure 7(b) is the adjusted clear-sky fluxes, labeled BERMS-clear, which were then used to calculate α_{cloud} for the BERMS data from (2). The few data points in winter in Figure 7(b), which are

still above the clear-sky envelope were rejected as bad data, probably caused by ice lenses on the pyranometer. For these we set α_{cloud} =0.05, based on comparisons with α_{cloud} derived from the photosynthetically active radiation (PAR) data (not shown). The incompatibility between the BERMS SW measurements and the ERA-40 clear-sky fluxes in winter does introduces some uncertainty into the comparison of α_{cloud} between model and data in these winter months.

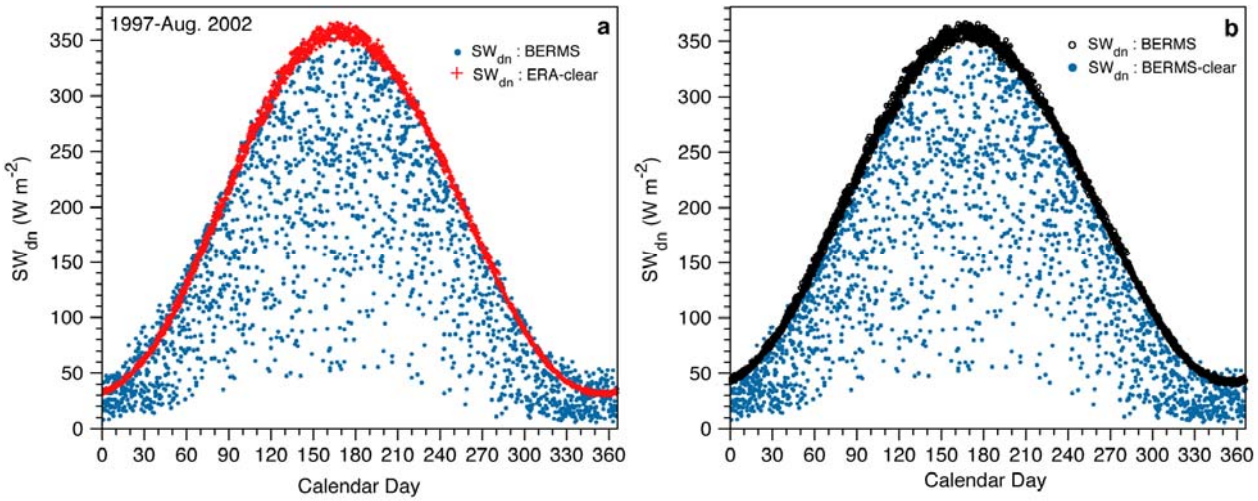

Figure 7a) BERMS mean daily SW_{dn} and SW_{dn}(ERA-clear); b) BERMS SW_{dn} and clear-sky flux from (A3).

4.3 Comparison of $\forall_{cloud}$ from BERMS sites and ERA-40

Figures 8(a) and (b) plot α_{cloud} derived from the SW_{dn} at OJP and OA against OBS, together with the regression lines. As expected, the correlation is higher for the closest sites. Although α_{cloud} is determined from $SW_{dn,}$ the correlations are lower than in Figures 7(a) and (b) because the range of variability of α_{cloud} is smaller, only from 0 to 1. Figure 8(c) plots α_{cloud} for the ERA-40 point against the BERMS mean α_{cloud}, computed from the BERMS mean of the SW_{dn} flux. The correlation is poor. Clearly we can determine a BERMS mean α_{cloud} on a daily basis far better than ERA-40 can predict it. Given this large scatter in α_{cloud} on the daily timescale, we must average to assess the model biases, and we first look at the mean seasonal cycle.

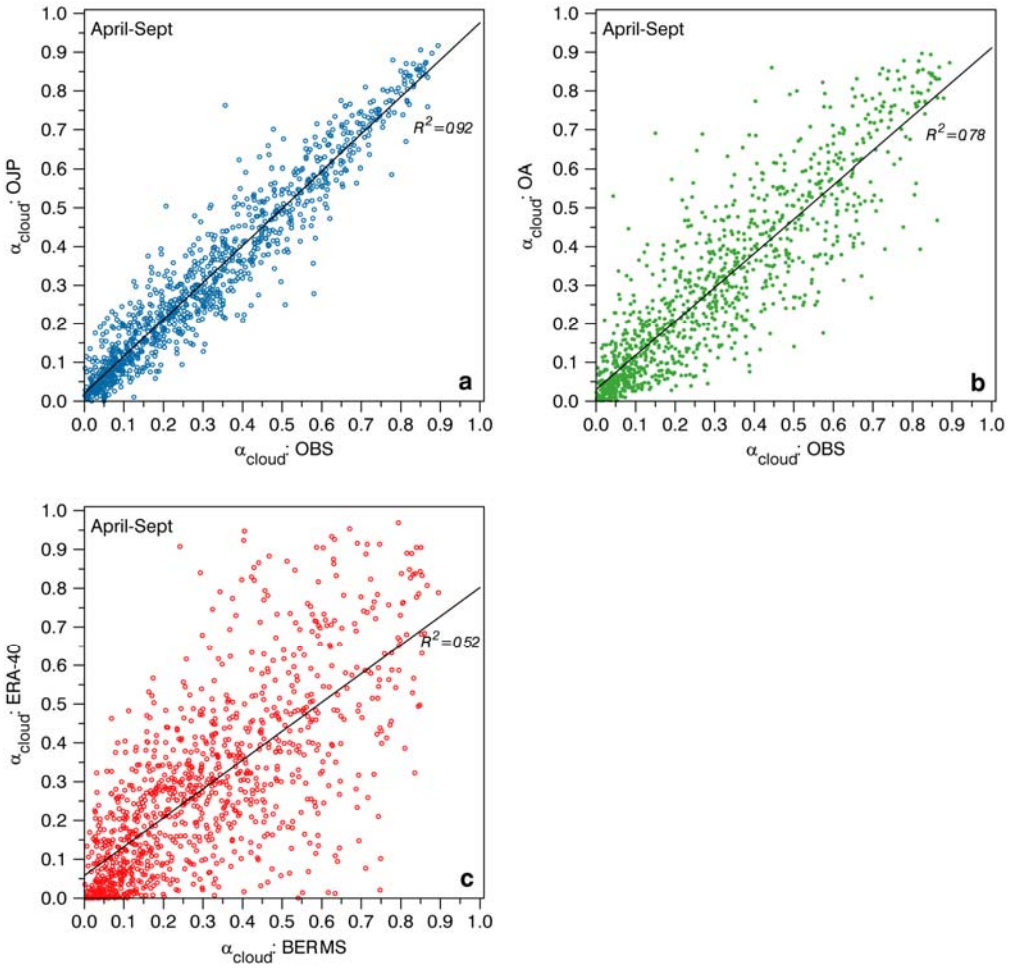

Figure 8a) Comparison of α_{cloud} at OJP with OBS, b) As a) for OA, c) ERA-40 plotted against BERMS mean α_{cloud}.

4.4 Seasonal cycle comparison of BERMS sites and ERA-40

Figure 9a shows monthly averages of cloud albedo (upper curves) and surface albedo (lower curves) for the three BERMS sites, and ERA-40 (heavy line). For α_{cloud} the BERMS sites are very similar with peaks in cloud in June when the number of days with α_{cloud} <0.2 sharply decreases, and in November when the number of days with α_{cloud} >0.6 peaks. ERA-40 has a lower cloud albedo than the data in all months except July. In spring, fall and winter, ERA-40 simply has more days of low cloud albedo and fewer days of high cloud albedo (not shown). The differences in surface albedo for the different forest canopies are larger than the differences in the cloud albedo (characteristic of the atmosphere). OJP has a higher albedo than OBS throughout the year and OA has the highest albedo, both in winter with snow (the most open canopy) and in summer when in leaf. In the surface energy budget, however, the cloud albedo and its daily and seasonal variability plays a larger role than the variations in the surface albedo. The ERA-40 albedo lies above that of the conifer sites for most of the year.

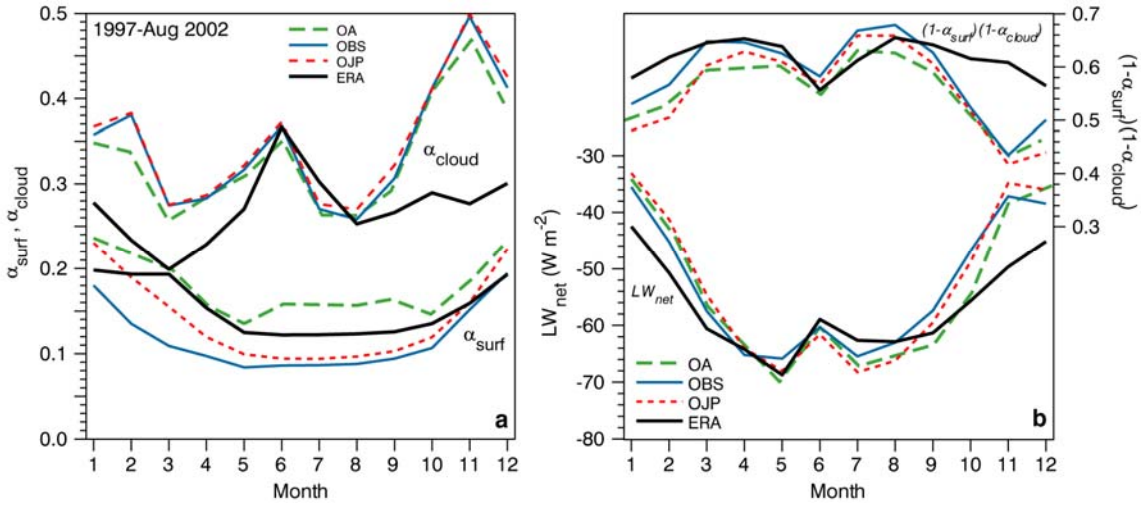

Figure 9: Seasonal cycle of a) Cloud albedo and surface albedo b) SW_{net} and LW_{net} for the three BERMS sites and ERA-40.

Figure 9b has two sets of curves. The upper set is the scaled $SW_{net,}$ given by (3), showing that for the data the OBS site has the highest scaled SW_{net}, because it has the lowest surface albedo. ERA-40 is higher than the data in winter, because of its lower cloud cover. The lower curves are LW_{net}, which show that despite the small differences in near-surface T, RH and atmospheric cloud cover, the differences in LW_{net} between BERMS sites on a seasonal timescale are relatively small, only a few W m^{-2}. ERA-40 has a larger outgoing LW_{net} in winter, which is consistent with its lower cloud cover.

4.5 Seasonal cycle of sensible and latent heat fluxes for BERMS and ERA-40

We have data for H and λE for all three BERMS sites and ERA-40 for September, 1999 - August, 2002, so we shall compare the mean seasonal cycles for just this three-year period. Figure 10a compares the monthly averages of the surface sensible and latent heat fluxes for the three sites with ERA-40 (heavy lines). H (the group of curves to the left) is negative in mid-winter, and rises steeply from January to May when evaporation is low. For this period, the ERA-40 sensible flux is lower than the three forest sites, which are almost identical. OBS and OJP have slightly greater H, probably because their surface albedo is lower. After leaf-out, H at OA falls well below OBS and OJP, which remain similar for most of the year (this is also true on the daily time-scale, not shown). The group of curves to the right is 8λ, which peaks in July at all three sites, with the deciduous forest OA>OBS>OJP as expected. For ERA-40, λE is as large as at OA in mid-summer, much greater than at the conifer sites. The residual in the surface energy balance at the BERMS sites for the period April to July is significant, about 15% of R_{net}, while the measured storage is small: G/R_{net} ≈ 4%. In contrast, for the same period, ERA-40, which has no residual, has a larger storage term (G/R_{net} ≈ 17%), which includes a phase change term as the soil melts in spring. As a result, the differences between ERA-40 and the BERMS sites in the sum (H + λE) in the surface energy balance (1) are small.

Figure 10b shows the seasonal cycle of R_{net} and EF, recomputed from the monthly mean fluxes, and shown only from March to October. For $R_{net,}$ the net flux decreases in the sequence OBS, OJP to OA in summer, because of the differences in surface albedo. ERA-40 has some differences from the BERMS sites, associated with the differences in cloud cover and LW_{net}. Note than in winter, when cloud cover is lower in

the reanalysis, ERA-40 has lower values of R_{net} and H than the BERMS sites by about -10 Wm^{-2} in January. This appears to be inconsistent with the small warm bias in ERA-40 in winter shown in Figure 4a, suggesting other compensating processes in the model, such as the larger fluxes from the ground in winter (Viterbo et al., 1999). The pattern of EF for the BERMS sites is as expected: OBS is above OJP and both rise monotonically from March to August; while OA has a much higher narrower peak, as EF rises and falls steeply with leaf-out and senescence. In contrast, EF for ERA-40 is above the conifer sites, which dominate the landscape (Barr et al., 1997) from March to October, and is only a little smaller than OA in summer. It is likely that ERA-40 has too small H and too large 8E and therefore too large EF throughout the year. In the cool season this is clearly the lack of a seasonal cycle in the vegetation in the model; while in summer, the details of the stomatal conductance formulation (Van den Hurk et al., 2000) may need revision.

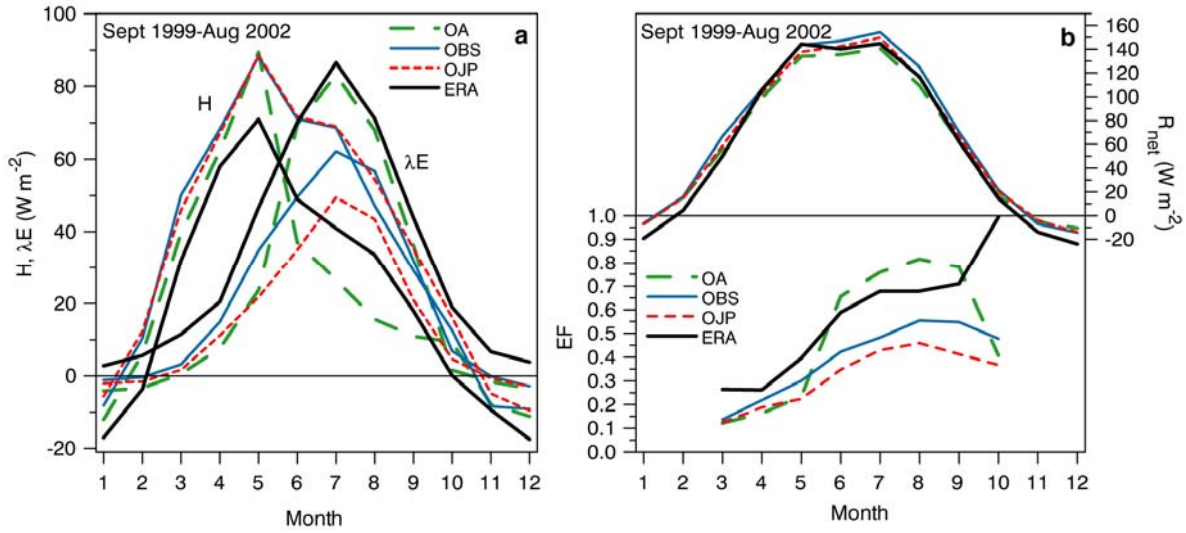

Figure 10: Seasonal cycle of a) H and λE and b) R_{net} and EF for OA, OBS, OJP and ERA-40.

Given the large differences in the surface energy flux partition between the different forest sites shown in Figure 10, and the heterogeneity of the landscape which includes lakes, fens, recent burns, disturbed and regenerating areas and mixed forest (for which we have no data), we cannot generate a true landscape mean for H and λE for BERMS. However, a simple mean of the three sites is again useful to look at the structure of the ERA-40 biases in more detail.

4.6 ERA-40 biases as a function of BERMS cloud albedo

We now partition the daily data between April-September for the (ERA-40-BERMS) differences in bins of the BERMS cloud albedo. Figure 11(a) shows that when large cloud cover is observed, ERA-40 has a negative bias in α_{cloud} and a corresponding bias in LW_{net}. When observed cloud cover is small, the biases of ERA-40 are reversed, and they are smaller. Note that the standard deviations of model daily biases are large because of the large scatter in α_{cloud} shown in Figure 8(c). Figure 11(b) is the corresponding plot for the ERA-40 bias in T and RH. As BERMS α_{cloud} increases, ERA-40 shifts from having a cool, moist bias with too much cloud to a warm, dry bias with too little cloud. Figure 11(c) shows a subset of the data; extracted from the three years, September 1999-August 2002 for which we have both observations of H and λE and the ERA-40 model data. On the left-hand-scale, we show the ERA-40 bias of α_{cloud}, and on the right-hand-scale

the differences of the ERA-40 daily surface fluxes from the mean of the three BERMS sites. We will refer to this as an ERA-40 bias, even though we not have a true landscape mean for BERMS. A few representative standard deviations of the daily biases are shown: these are again large. Latent heat flux in ERA-40 has a high bias of order10 Wm^{-2} across all cloud cover; and ERA-40 has a 2% higher surface albedo (not shown) which contributes about -5 Wm^{-2} to the R_{net} bias. The ERA-40 bias of α_{cloud} is projected onto a bias of R_{net} and H. When observed cloud cover is low, ERA-40 has too much cloud giving low R_{net} and H, which gives a cold, moist bias, since 8E has always a high bias. When observed cloud cover is high, the pattern reverses: ERA-40 has too little cloud, R_{net} and H are high, giving a warm, dry bias. One caveat should be noted. The panels in Figure 11 suggest that the bias of cloud cover on individual days is the physical link that connects all the other biases. This is consistent with the analysis that we present in the next section. However, the bias pattern itself, which has large error bars, is in part created by the binning from Figure 8(c), where the correlation of α_{cloud} between ERA and BERMS is poor.

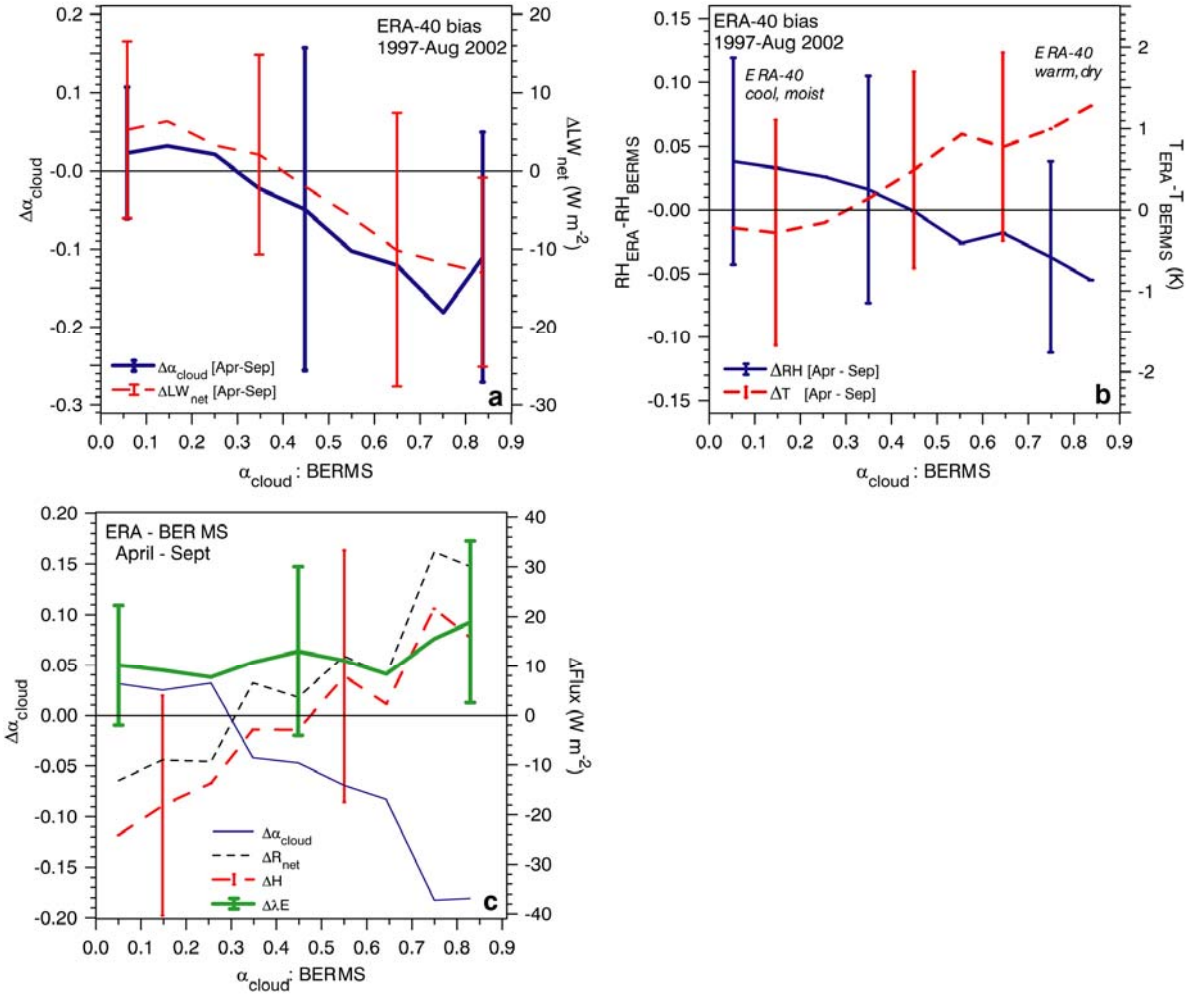

Figure 11: Stratification by mean BERMS α_{cloud} for a) ERA-40 biases of cloud albedo and LW_{net} b) as (a) for ERA-40 biases of T and RH (c) ERA-40 surface flux biases.

5. Surface -BL - cloud coupling in summer

In this section we ask whether the reanalysis represents on the daily timescale the coupling of processes that is seen in data. This also gives insight into the links in the coupled system. Because we are not looking primarily at biases and we need the largest data sample possible, we will take the five summers of the BERMS data (June, July and August, 2000-2004), and for ERA-40, the five summers of 1998-2002.

5.1 Stratification of data by $\forall_{cloud}$

Figure 12 compares the surface energy balance for the BERMS sites and ERA-40, averaged in 0.1 bins of α_{cloud} (BERMS mean or ERA-40). Panel(a) shows SW_{net}, R_{net} and LW_{net} and RH (on right-hand-scale). The radiation fluxes and RH are quasi-linear in cloud cover, which has a linear impact on SW_{net} (from (3)), and also the quasi-linear impact on LW_{net} seen here for small $\alpha_{cloud,}$ OBS>OJP>OA for SW_{net} and R_{net}, with ERA-40 in between. The differences in the radiation fluxes, and the near-surface RH (related to P_{LCL}) between data and model are very small. This means the coupling between BL parameters, the cloud field and the radiation field appears similar in data and model. Because RH and α_{cloud} have a quasi-linear relationship, the stratification of the data by RH gives a similar perspective (not shown).

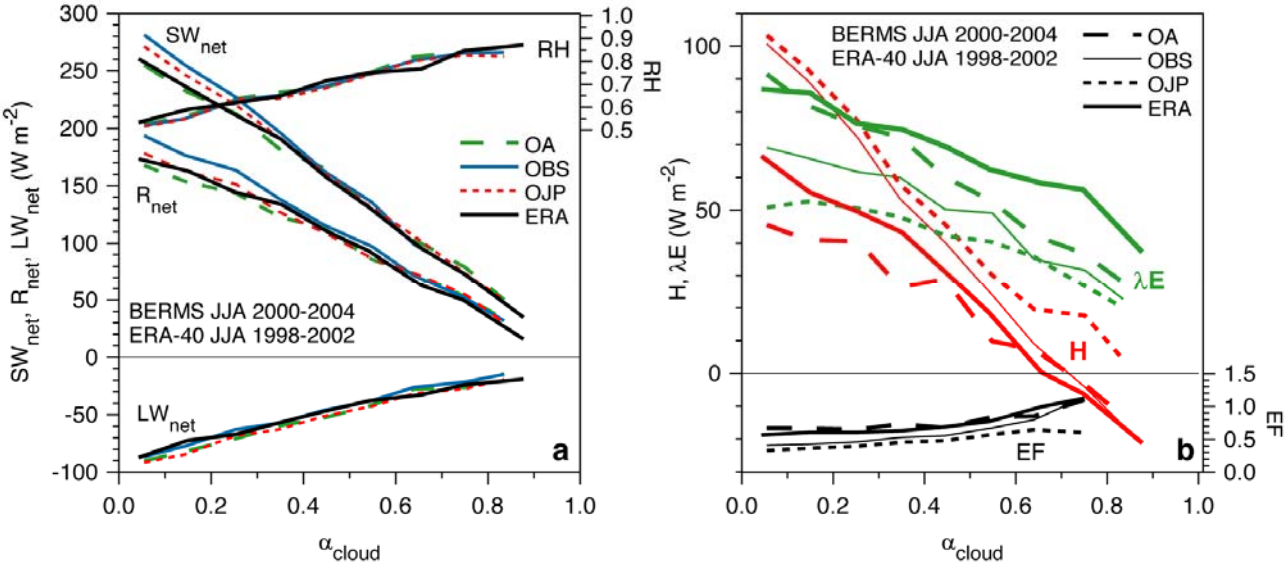

Figure 12a) Net radiative fluxes and RH as functions of α_{cloud} for BERMS sites and ERA-40, b) As (a) for H (red), λE (green) and EF.

Panel b) is the corresponding plot for H, λE and EF (right-hand-scale). Here we see considerable differences between the model and the different BERMS sites. For each site the (H, λE) pairs reflect the sequence of EF with OA>OBS>OJP. At low cloud cover, EF for ERA-40 is less than at OA, but when cloud cover is high, ERA-40 has more evaporation and a higher EF than any of the BERMS sites. Generally H falls more steeply with α_{cloud} than does λE, although for OA the two slopes are similar. At high cloud cover, when the canopy, moss and understory are often wet with precipitation, H becomes negative for OA, OBS and ERA-40, while OJP diverges from OBS. The ground heat storage in ERA-40 is significantly higher than in BERMS, except at high cloud cover, but BERMS has a roughly 20 W m^{-2} residual in the SEB which increases slightly with cloud cover (not shown). The relatively weak dependence of λE on α_{cloud} in the coupled system is significant

and several physical processes are involved. At low cloud cover, direct radiation is high and the canopy light response saturates, T will be higher and RH is lower, and these are stress factors for transpiration. High cloud is coupled also with precipitation and additional evaporation off wet canopies, the understory and moss layer (where present). The steeper slope for H than λE in Fig. 12(b) suggests that H is more tightly coupled to R_{net} than is λE, which is consistent with Figure 11(c). The standard deviations in Figure 12 are partly determined by the 0.1 albedo bin size, which gives a range for SW_{net}. Representative standard deviations for (H, λE, LW_{net}) are (20, 15, 12) Wm^{-2} and 0.12 for RH.

5.2 Interrelation of RH, α_{cloud} and LW_{net}

Despite the difference in the surface flux partition, the links of BL parameters, RH (and P_{LCL}), with α_{cloud} and LW_{net} (the important LW forcing at the surface) are essentially identical in the BERMS-mean and ERA-40, as shown in Figure 13. Thus cloud cover increases with RH, as mean cloud-base, P_{LCL}, decreases, and both these changes reduce the outgoing LW_{net} flux. Some representative standard deviations of the daily data are shown: note that they are smaller for LW_{net} than for cloud albedo.

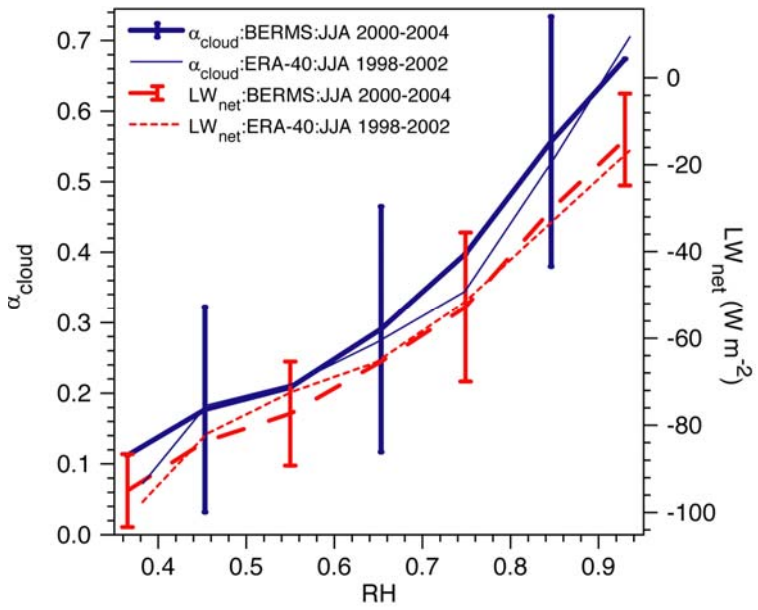

Figure 13: α_{cloud} and LW_{net} as a function of RH for BERMS and ERA-40.

Figure 14 partitions the relationship of LW_{net} to RH, seen in Figure 13, into four ranges of α_{cloud}. For this finer stratification of the data, we have increased the sample size to eight summers for BERMS and ten for ERA-40 (since we have these model data). This relationship is essentially identical for BERMS and ERA-40. Outgoing LW_{net} falls with both increasing cloud cover and increasing RH, which corresponds to a shallower mean sub-cloud layer, P_{LCL}. With this further partition, the standard deviation of the daily data falls to about 10 W m^{-2} (representative sets are shown). Betts and Viterbo (2005) showed a similar pattern for ERA-40 for a sub-basin of the Amazon.

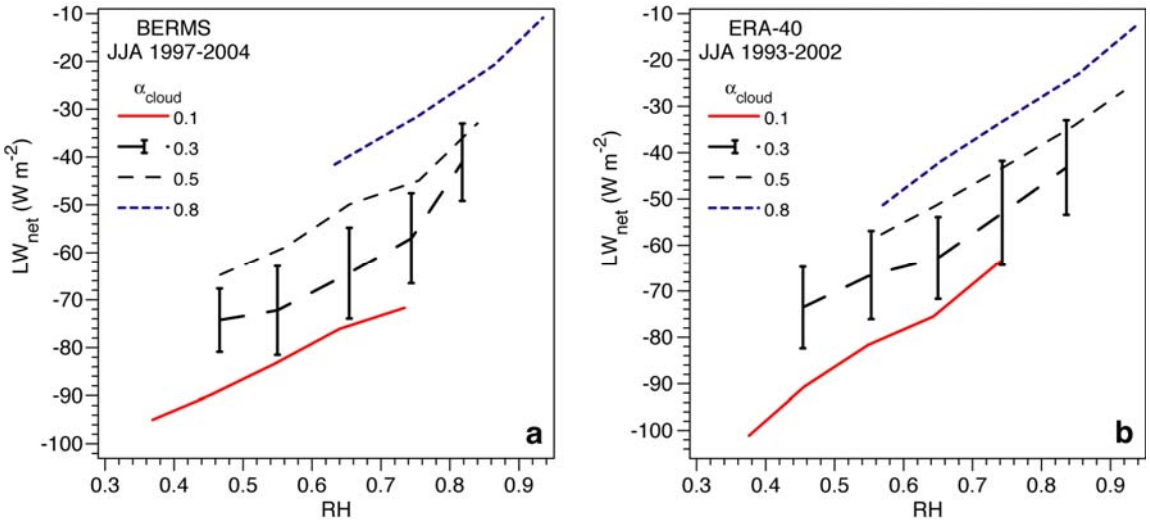

Figure 14: LW_{net} as a function of RH and α_{cloud} for a) BERMS and b) ERA-40.

5.3 Influence of soil moisture

A characteristic of the ERA-40 land-surface model (Van den Hurk et al., 2000) and its predecessor (Viterbo and Beljaars, 1995) is that because stomatal resistance is a function of soil water, soil water is linked to both evaporation and to daily-mean near-surface RH and P_{LCL}, as shown in Figure 15 for the months June, July and August. The abscissa, SWI:0-7cm, is the available soil water index for the first model soil 7-cm layer (which runs from 0 to 1 between the permanent wilting point and field capacity of the model soil). Note that it can exceed unity after recent rain. RH increases and LCL decreases with soil water index and also with α_{cloud}. The heavy line is the mean of all the data, and a representative set of standard deviations is shown on one sub-class of cloud albedo. Note that for this boreal forest region, soil water in the model is relatively high in summer. This link between SWI, RH and the LCL (and EF, not shown) has been a characteristic of the ECMWF model for some years (Betts et al, 1998b, 1999b, Betts, 2004; Betts and Viterbo, 2005). Some evidence for this link exists in data (Betts and Ball, 1998; Dirmeyer et al., 2005). Over the boreal forest, stomatal control on transpiration is strong and soils are heterogeneous. The wide-spread organic soils (characteristic of OBS) are usually moist, and soil water has less of a control on evaporation. Often the availability of water for evaporation depends significantly on water stored in a surface moss layer (Price et al., 1997; Betts et al., 1999a). At OJP, transpiration depends on soil water, but in the sandy soil drainage is relatively rapid (Cuenca et al., 1997; Joiner et al., 1999). The BERMS sites have volumetric soil moisture measurements, both shallow (0-10 cm) and throughout the rooting depth (to depths of 120 cm at SOA, 60 cm at SOBS and 150 cm at SOJP). However, we cannot evaluate Figure 15, since a representative regional mean cannot be constructed from these point data.

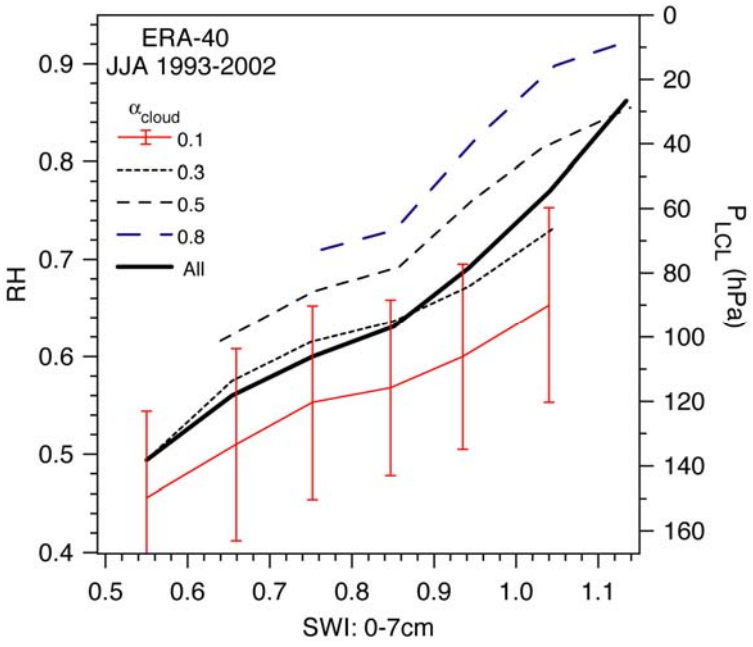

Figure 15: Near-surface RH (and P_{LCL}) as a function of ERA-40 0-7cm available soil water and α_{cloud}.

5.4 Discussion of ERA-40 biases

Our analysis shows the links between variables in the coupled system, but generally cause and effect are not obvious. However, since we wish to improve the analysis and forecast model, it is necessary to speculate where the sources of error may lie, as this suggests possible sensitivity studies with the model physics. The primary biases we have noted are in 8E, EF and α_{cloud}. ERA-40 specifically appears to have a positive bias in 8E for all α_{cloud}. Here it is likely that the primary cause lies in the land-surface model formulation of evaporation, rather than atmospheric or cloud related processes. Perhaps the vegetative conductance, which depends on soil water, radiation and RH stress functions is too high. The model lacks a seasonal vegetation cycle, which gives a high bias of evaporation in spring and fall; and the soil water analysis increments (Douville et al., 2000) provide water in summer (Betts et al., 2003), and prevent high λE from drying out the soil. During and after rain, perhaps the evaporation from the wet model canopy is too high. However, the RH is a balance between the surface fluxes and the exchanges between the BL and the atmosphere above, including the evaporation of falling precipitation (which cools and moistens into the sub-cloud layer, and reduces the surface evaporation). Figure 12 is puzzling in that, for very similar values of RH and α_{cloud}, evaporative fraction in ERA-40 is generally higher than the BERMS data, especially at high cloud cover. This suggests that the same BL equilibrium is being maintained in ERA-40 in the face of higher EF by differences in the vertical exchanges with the atmosphere above. For example, the model might have too high an exchange of warm dry air from above the BL or too little evaporation of falling precipitation; but these possibilities can only be tested with model sensitivity studies.

Except in summer, ERA-40 tends to have too little reflective cloud. On days that are observed to be cloudy, ERA-40 has a low bias in α_{cloud}; and on these days a tendency to a warm, dry bias in the BL, despite the positive bias in surface 8E (Figures 11 and 12). This suggests the source of this model error may be in the formulation of cloud processes in the atmosphere, but we cannot say where. It could be in the cloud

generation parameterizations, or once again the warm, dry bias in the BL could be related to too little evaporation of falling precipitation below cloud-base. In summer, this same bias (of too little cloud on disturbed days) occurs, but there is a compensating bias on other days. When observed cloud cover is <50%, ERA-40 has a tendency towards a positive α_{cloud} bias, and an associated cool, moist bias near the surface. As these are the less disturbed days, the links here could all be in the surface-BL coupling, which are quite strong in the model (Betts and Viterbo, 2005); with excessive evaporation being linked to a cool, moist sub-cloud layer, more BL cloud, and less R_{net}, which reinforces the lower surface sensible heat flux (Figure 11).

6. Conclusions

Using daily averaged data we have intercompared the three mature BERMS sites in central Saskatchewan with each other and with a single close-by grid-point from the ERA-40 reanalysis. On the seasonal timescale the ERA-40 biases in T and RH are small. Data at the two conifer sites, OBS and OJP, only 29km apart, are highly correlated on a daily time-scale. The correlation with the deciduous aspen site 81km away is reduced, but still greater than the correlation of any BERMS site with the ERA-40 time-series. Consequently, we felt justified in averaging the three BERMS sites for comparison with the reanalysis. This is satisfactory for T and RH as well as for the downward and net radiation fields. Because cloud cover plays such an important role in the surface energy budget, we computed a cloud albedo from both model and BERMS data to represent the SW cloud forcing at the surface. On a seasonal timescale, ERA-40 has a lower cloud albedo and a higher SW_{net} flux than BERMS in all months except July. ERA has a larger outgoing LW_{net} in the cold season, which is consistent with its lower cloud cover. The resulting bias in R_{net} is small on a seasonal timescale, except in winter. The ERA-40 land-surface model classifies this grid-point as 97.6% evergreen needleleaf trees, but the model evaporation is greater than the conifer sites throughout the year and comparable to the deciduous aspen site in the growing season. Given the heterogeneity of the landscape, we cannot compute a true landscape mean for the surface H and λE from these three old growth stands, but we did use a simple mean of the three BERMS sites to look at the structure of the ERA-40 biases of H and λE. We stratified the ERA-40 biases by both observed BERMS RH and α_{cloud}. In the warm season, ERA-40 has a cool, moist bias with too much cloud (when BERMS α_{cloud} is small); and this reverses when observed cloud cover is high to a warm dry bias with too little cloud in ERA-40, and a corresponding bias in R_{net}. The model high bias in λE (from April to September) is independent of cloud cover, so that the bias of the model cloud cover and R_{net} is projected onto a bias of H.

We then asked whether the model represents the coupling of processes that is seen in nature on the daily timescale; specifically, the relationships between surface fluxes and RH and α_{cloud}. All the components of the surface energy balance are quasi-linear when stratified by α_{cloud}. $SW_{net,}$ outgoing $LW_{net,}$ R_{net} and sensible heat flux fall steeply with increasing α_{cloud}, but latent heat flux falls only weakly for OBS, OJP and ERA-40. In this stratification, the radiation fluxes and RH differ little between data and reanalysis, with the primary difference being that ERA-40 has a much higher EF than the conifer sites. The important outgoing LW_{net} falls with both increasing cloud cover and increasing RH, (corresponding to a shallower sub-cloud layer in the mean), and this relationship is essentially identical for the BERMS-mean and ERA-40. ERA-40 has a strong coupling between soil water, RH and cloud cover in summer, but we cannot evaluate this using the BERMS soil water measurements.

The biases of ERA-40 over the boreal forest are encouragingly small on a seasonal timescale. Perhaps this is not too surprising since data from the BOREAS was used in the development of its land-surface model (Van den Hurk et al., 2000, Betts et al., 2001). The BERMS data, which did not enter the reanalysis, are of high quality and of sufficient length to be extremely useful in identifying residual biases in the land-surface interaction in the ERA-40. Our analysis shows the links between variables in the coupled system, but generally cause and effect are not obvious, and model sensitivity studies will be needed to identify possible improvements to the model physical parameterizations.

Acknowledgments

Alan Betts acknowledges support from NSF under Grant ATM05-29797 and from NASA under NEWS grant NNG05GQ88A. The BERMS data collection has been supported by the Meteorological Service of Canada and Fluxnet-Canada (with support from the Natural Sciences and Engineering Research Council of Canada, the Canadian Foundation for Climate and Atmospheric Science, and Biocap Canada). We thank Zoran Nesic, Kai Morgenstern, Andrew Sauter, Joe Eley, Dell Bayne, Erin Thompson, Charmaine Hrynkiw and Steve Enns for assistance in field measurements and data management. Two excellent reviews have greatly improved the paper.

References

Amiro, B.D., A.G. Barr, T.A. Black, H. Iwashita, N. Kljun, J.H. McCaughey, K. Morgenstern, S. Murayama, Z. Nesic, A.L. Orchansky, and N. Saigusa, 2005. Carbon, energy and water fluxes at mature and disturbed forest sites, Saskatchewan. Canada. *Agric. For. Meteorol*. **136**, 237-251.

Amiro, B.D., A.L. Orchansky, A.G. Barr, T.A. Black, S.D. Chambers, F.S. Chapin III, M.L. Goulden, M. Litvak, H.P. Liu, J.H. McCaughey, A. McMillan and J.T. Randerson, 2006. The effect of post-fire stand age on the boreal forest energy balance. *Agric. For. Meteorol*. (in press).

Arain, A., T.A. Black, A.G. Barr, P.G. Jarvis, J.M. Massheder, D.L Verseghy and Z. Nesic, 2002. Effects of seasonal and interannual climate variability on net ecosystem productivity of boreal deciduous and conifer forests. *Can. J. Forest Research*, **32**, 878-891.

Arain, M.A., Black, T.A., Barr, A.G., Griffis, T.J., Morgenstern, K and Nesic, Z., 2003. Year round observations of the energy and water vapour fluxes above a boreal black spruce forest. *Hydrological Processes*, **17**, 3581-3600.

Baldocchi, D.D., C.A. Vogel, and B. Hall, 1997. Seasonal variation of energy and water vapor exchange rates above and below a boreal jack pine forest canopy. *J. Geophys. Res*., **102,** 28939-28952.

Barr, A.G. A.K. Betts, R. Desjardins and J. I. MacPherson, 1997. Comparison of regional surface fluxes from boundary-layer budgets and aircraft measurements above boreal forest. *J. Geophys. Res*., **102**, 29213-29218.

Barr, A.G., G. van der Kamp, R. Schmidt and T. A. Black, 2000. Monitoring the moisture balance of a boreal aspen forest using a deep groundwater piezometer. *Agric. For. Meteorol*., **102,** 13-24.

Barr, A.G., T.J. Griffis; T.A. Black, X. Lee, R.M. Staebler, J.D. Fuentes, Z. Chen and K. Morgenstern, 2002. Comparing the carbon balances of boreal and temperate deciduous forest stands. *Can. J. Forest Research*, **32,** 813-822.

Barr, A.G., Black, T.A., Hogg, E.H., Kljun, N., Morgenstern, K., Nesic, Z., 2004. Inter-annual variability in the leaf area index of a boreal aspen-hazelnut forest in relation to net ecosystem production. *Agric. For. Meteorol*., **126,** 237-255.

Barr, A.G., T.A. Black, E.H. Hogg, T. Griffis, K. Morgenstern, N. Kljun, A. Theede and Z. Nesic, 2006. Climatic controls on the carbon and water budgets of a boreal aspen forest. 1994–2003 *Global Change Biology*, Published article online: 7-Aug-2006 doi: 10.1111/j.1365-2486.2006.01220.x

Betts, A. K., 2004. Understanding hydrometeorology using global models. *Bull. Amer. Meteorol. Soc*., **85**, 1673-1688.

Betts A. K. and J. H. Ball, 1998. FIFE surface climate and site-average dataset:1987-1989. *J. Atmos Sci*., **55,** 1091-1108.

Betts, A. K and P. Viterbo, 2005. Land-surface, boundary layer and cloud-field coupling over the south-we stern Amazon in ERA-40. *J. Geophys. Res*., **110**, D14108, doi:10.1029/2004JD005702.

Betts A. K., P. Viterbo, A.C.M. Beljaars, H-L. Pan, S-Y. Hong, M. L.Goulden and S.C. Wofsy, 1998a. Evaluation of the land-surface interaction in the ECMWF and NCEP/NCAR reanalyses over grassland (FIFE) and boreal forest (BOREAS). *J. Geophys. Res*., **103**, 23079-23085.

Betts, A. K., P. Viterbo and E. Wood, 1998b. Surface energy and water balance for the Arkansas-Red river basin from the ECMWF reanalysis. *J. Climate*, **11**, 2881-2897.

Betts, A. K., M. L. Goulden, and S.C. Wofsy, 1999a. Controls on evaporation in a boreal spruce forest. *J. Climate*, **12**, 1601-1618.

Betts, A. K., J.H. Ball and P. Viterbo, 1999b. Basin-scale surface water and energy budgets for the Mississippi from the ECMWF Reanalysis. *J. Geophys. Res*., **104**, 19293-19306.

Betts , A. K.,, P. Viterbo, A.C.M. Beljaars and B.J.J.M. van den Hurk, 2001. Impact of BOREAS on the ECMWF Forecast Model. *J. Geophys. Res*., **106**, 33593-33604.

Betts, A. K., J. H. Ball and P. Viterbo, 2003. Evaluation of the ERA-40 surface water budget and surface temperature for the Mackenzie River basin. *J. Hydrometeorology*, **4**, 1194-1211.

Betts, A. K., R. Desjardins and D. Worth, 2006a. Impact of agriculture, forest and cloud feedback on the surface energy balance in BOREAS. *Agric. Forest Meteorol*., doi:10.1016/j.agrformet.2006.08.020

Betts, A.K., M. Zhao, P. A. Dirmeyer and A.C.M. Beljaars, 2006b. Comparison of ERA40 and NCEP/DOE near-surface datasets with other ISLSCP-II datasets. *J. Geophys. Res*. 111, D22S04, doi:10.1029/2006JD007174.

Black, T.A., Chen, W.J., Barr, A.G., Arain, M.A., Chen, Z., Nesic, Z., Hogg, E.H., Neumann, H.H., and Yang, P.C., 2000. Increased carbon sequestration by a boreal deciduous forest in years with a warm spring. *Geophys. Res. Lett*. **27**, 1271-1274.

Blanken, P.D., T.A. Black, P.C. Yang, H.H. Neumann, Z. Nesic, R. Staebler, G. den Hartog, M.D. Novak, and X. Lee, 1997. Energy balance and canopy conductance of a boreal aspen forest: partitioning overstory and understory components. *J. Geophys. Res*.,**102**, 28915-28927.

Blanken, P.D., T.A. Black, H. H. Neumann, G. den Hartog, P. C. Yang, Z. Nesic and X. Lee, 2001. The seasonal water and energy exchange above and within a boreal aspen forest. *Journal of Hydrology,* **245**(1-4), 118-136.

Chen, J.M., W. Ju, J. Cihlar, B. Amiro, D. Price, J. Liu, W. Chen, J. Pan, A. Black, and A. Barr, 2003. Spatial Distribution of Carbon Sources and Sinks in Canada's Forests Based on Remote Sensing, *Tellus*, **55B**, 622-641.

Cuenca, R. H., D.E. Stangel, and S.F. Kelly, 1997. Soil water balance in a boreal forest. *J. Geophys. Res*., **102**, 29,355-29,365.

Dirmeyer, P. A., R. D. Koster, and Z. Guo, 2006. Do global models properly represent the feedback between land and atmosphere? COLA Technical Report 192, 47 pp; *J. Hydrometeor.* (in press).

Douville, H., P. Viterbo, J.-F. Mahfouf, and A.C.M. Beljaars, 2000. Evaluation of optimal interpolation and nudging techniques for soil moisture analysis using FIFE data, *Mon. Wea. Rev*., **128**, 1733-1756.

Drolet, G.G., K.F. Huemmrich, F.G. Hall, E.M. Middleton, T.A. Black, A.G. Barr, and H.A. Margolis, 2005. A MODIS-derived photochemical reflectance index to detect inter-annual variations in the photosynthetic light-use efficiency of a boreal deciduous forest. *Remote Sensing of the Environment*. **98**, 212-224.

Grant, R.F., Zhang, Y., Yuan, F., Wang S., Gaumont-Guay, D., Hanson, P.J., Chen, J., Black, T.A., Barr, A., Baldocchi D.D. and Arain A., 2005. Modelling water stress effects on CO2 and energy exchange in temperate and boreal deciduous forests. *Global Biogeochemical Cycles* (in press).

Griffis, T.J., T.A. Black, K. Morgenstern, A.G. Barr, Z. Nesic, G. Drewitt, D. Gaumont-Guay, and J.H. McCaughey. 2003. Ecophysiological controls on the carbon balances of three southern boreal forests. *Agric. For. Meteorol*. **117**, 53-71.

Griffis, T.J., Black, T.A., Gaumont-Guay, D., Drewitt, G.B., Nesic, Z., Barr, A.G., Morgenstern, K. and Kljun, N. 2004. Seasonal variation and partitioning of ecosystem respiration in a southern boreal aspen forest. *Agric. For. Meteorol.*, **125**, 207-223.

Jarvis, P. G., 1976. The interpretation of the variations of leaf-water potential and stomatal conductance found in canopies in the field. *Philos. Trans. Roy. Soc. London*, **B723**, 593-610.

Jarvis, P. G., J. M. Massheder, S. E. Hale, J. B. Moncrieff, M. Rayment and S. L. Scott, 1997. Seasonal variation of carbon dioxide, water vapor, and energy exchanges of a boreal black spruce forest, *J. Geophys. Res.*, **102**, 28953-28966.

Joiner, D. W., J. H. McCaughey, P. M. Lafleur, and P.A. Bartlett, 1999. Water and carbon dioxide exchange at a boreal Young Jack Pine site in the BOREAS northern study area, *J. Geophys. Res*., **104**, 27,641-27,652.

Ju, W., J.M. Chen, T.A. Black, A.G. Barr, J.H. McCaughey, and N. Roulet, 2006. Hydrological Effects on Carbon Cycles of Canada's Forests and Wetlands. *Tellus* B, 58(1):16-30.

Kållberg, P., A. Simmons, S. Uppala and M. Fuentes, The ERA-40 archive. *ERA-40 Project Report*, *No. 17*, 31pp., Available from: http://www.ecmwf.int/publications/

Kljun, N., T.A. Black, T.J. Griffis, A.G. Barr, D. Gaumont-Guay, K. Morgenstern, J.H. McCaughey and Z. Nesic, 2006. Response of net ecosystem productivity of three boreal forest stands to drought. *Ecosystems* (in press)

Koster, R. D., et al. (2004), Regions of anomalously strong coupling between soil moisture and precipitation, *Science*, **305**, 1138–1140.

Pinker, R. T. and 13 co-authors, 2003. Surface radiation budgets in support of the GEWEX Continental-Scale International Project (GCIP) and the GEWEX Americas Prediction Project (GAPP), including the North American Land Data Assimilation System (NLDAS) project, *J. Geophys. Res*., **108**(D22), 8844, doi:10.1029/2002JD003301.

Price, A. G., K. Dunham, T. Carleton, and L. Band, 1997. Variability of water fluxes through the black spruce (Picea mariana) canopy and feather moss (Pleurozium schreberi) carpet in the boreal forest of northern Manitoba. *J. Hydrol.*, **196**, 310-323.

Uppala, S.M. and 45 co-authors, 2005. The ERA-40 Reanalysis. *Quart. J. Roy. Meteorol. Soc.*, **131**, 2961-3012.

Van den Hurk, B.J.J.M., P. Viterbo, A.C.M. Beljaars and A. K. Betts, 2000. Offline validation of the ERA40 surface scheme. *ECMWF Tech Memo, 295*, 43 pp. Available from: http://www.ecmwf.int/publications/

Viterbo, P. and A.C.M. Beljaars, 1995. An improved land-surface parameterization in the ECMWF model and its validation. *J. Climate*, **8**, 2716-2748.

Viterbo, P., A.C.M. Beljaars, J-F Mahfouf, and J. Teixeira, 1999. The representation of soil moisture freezing and its impact on the stable boundary layer. *Quart. J. Roy. Meteor. Soc*., **125**, 2401-2426.

Appendix: Reconciliation of measured SW_{dn} and model clear-sky fluxes in winter

We first weighted the ERA-40 clear-sky fluxes seasonally for the solar geometry for each of the BERMS sites, using an empirical fit

$$\text{SolarWT} = a + b\,[\cos(B\,DS/365)]6 \qquad \text{(A1)}$$

where DS is calendar days measured from the winter solstice. The coefficients a and b are given in Table A1. This is a small correction, which at the winter solstice, increases the clear-sky flux by 5.7, 6.6 and 10.7% for OBS, OJP and OA respectively. We then multiplied the clear-sky flux by an additional seasonal weighting function, the same for each site

$$\text{BERMSWT} = 1 + 0.25*(\cos(B*DS/365))^4 \qquad \text{(A2)}$$

to give a clear-sky flux,

$$\text{SWdn(BERMS-clear)} = \text{SolarWT}*\text{BERMSWT}*\text{SWdn(ERA-clear)} \qquad \text{(A3)}$$

The function, BERMSWT, is flat in mid-summer and increases the clear-sky fluxes by less than 1% for 55 days on either side of the summer solstice. In mid-winter, however, it increases the clear-sky flux by 25%, to make it consistent with the upper bound of the BERMS SW_{dn} fluxes, as shown in Figure 7(b). We then used (A3) in (2) to calculate α_{cloud} from the BERMS SW_{dn} data, for comparison with the corresponding α_{cloud} from the model.

Table A1. Weighting coefficients in (A1) for BERMS sites.

Site	a	b
OA	1.0034	0.104
OBS	1.0018	0.055
OJP	1.0021	0.064
BERMS mean	1.0024	0.074